Fast Plasma Shutdowns Obtained With Massive Hydrogenic, Noble and Mixed-Gas Injection in DIII-D

J.C. Wesley 1), E.M. Hollmann 2), T.C. Jernigan 3), M.A. Van Zeeland 1), L.R. Baylor 3), J.A. Boedo 2), S.K. Combs 3), T.E. Evans 1), M. Groth 4), D.A. Humphreys 1), A.W. Hyatt 1), V.A. Izzo 2), A. James 2), R.A. Moyer 2), P.B. Parks 1), D.L. Rudakov 2), E.J. Strait1), W. Wu 1), and J.H. Yu 2)

1) General Atomics, PO Box 85608, San Diego, California 92186-5608, USA
2) University of California-San Diego, La Jolla, California 92093, USA
3) Oak Ridge National Laboratory, Oak Ridge, Tennessee 37831, USA
4) Lawrence Livermore National Laboratory, Livermore, California 94550, USA

e-mail contact of main author: wesley@fusion.gat.com

Abstract. Massive gas injection (MGI) experiments with H_2, D_2, He, Ne and Ar and "mixed" (H_2 + Ar and D_2 + Ne) gases injected into "ITER-similar" 1.3-MA H-mode plasmas are described. Gas species, injected quantity Q, delivery time, t_{inj}, rate-of-rise and intrinsic and added impurities are found to affect the attributes and "disruption mitigation" efficacies of the resulting fast plasma shutdowns. With sufficient Q and $t_{inj} < \sim2$ ms, all species provide fast (within $\leq \sim3$ ms), more-or-less uniform radiative dissipation of the 0.7-MJ plasma thermal energy and fast but benign current decays with reduced vacuum vessel vertical force impulse. With pure and mixed low-Z gases, free-electron densities up to 2×10^{21} m^{-3} are obtained. While these densities are high relative to normal tokamak densities, they are still an order of magnitude smaller than the densities required for unconditional mitigation of the runaway electron avalanche process. Key information relevant to the design of effective MGI systems for larger tokamaks and ITER has been obtained and the collective species and Q-variation data provides a rich basis for validation of emerging 2D + t MHD/transport/radiation models.

1. Introduction

Pre-emptive injection of massive quantities ($\sim10^{22}$ atoms or molecules) of impurity and/or hydrogenic gas into an otherwise MHD-stable tokamak plasma has demonstrated the ability of massive gas injection (MGI) to produce a fast plasma thermal energy and current shutdown ("fast shutdown") that mitigates many adverse effects of naturally-occurring disruptions. "Disruption mitigation" benefits include: 1) rapid, more-or-less spatially-uniform radiation of the plasma thermal energy to the first wall, and 2) a fast plasma current decay that minimizes vertical instability, magnitude and toroidal asymmetry of in-vessel-component poloidal halo currents and magnitude of the vertical force on the torus vacuum vessel. In ITER, disruption thermal energy deposition on in-vessel surfaces and local and global halo-current-generated forces on in-vessel components and the vessel pose significant design and operational issues. Hence there are recognized needs for thermal energy deposition and halo-current and vessel-force mitigation and provision of a pre-emptive "disruption mitigation system" [1].

Injection of massive quantities of gas can also produce high free-electron densities, n_e, $\geq 10^{21}$ m^{-3}. The attainment of such high densities at onset of plasma current decay raises the prospect of using pre-emptive MGI to effect collisional suppression of the Coulomb-scattering ("knock-on") runaway electron avalanche [2]. However, as the analysis developed by Rosenbluth and others shows [1], free and/or total electron densities $\geq 10^{22}$ m^{-3} are needed for unconditional avalanche suppression in present tokamaks and ITER, and questions exist about the feasibility of obtaining and sustaining the very high electron densities needed for collisional mitigation of runaway avalanching during disruption or fast shutdown in ITER.

Characteristics of unmitigated disruptions and their consequential effects (including run-away avalanching) and the physics basis and status of candidate disruption mitigation methods, plus extensive references to experimental results and theoretical modeling are given in Refs. [1] and [3]. The results presented here comprise new experiments conducted in DIII-D, wherein an array of fast-opening gas injection valves was used to systematically investigate the effects of gas delivery attributes and species on the disruption and runaway electron mitigation attributes of pre-emptive fast plasma shutdowns. New understanding of how MGI attributes affect the feasibility of obtaining effective disruption and runaway avalanche mitigation in present tokamaks and in ITER has been obtained.

The balance of this paper is organized in six sections. Section 2 introduces the injection system, key diagnostics and attributes of the "ITER-similar" target plasmas used for the studies. The fast-shutdown phenomenology and characteristics common to the subsequent parametric data presentations are found here. Sections 3 through 6 respectively present how thermal energy mitigation, current decay and vessel force mitigation and added free and total electron densities and runaway electron generation and inferred avalanche mitigation depend on gas quantity, species and delivery rate. Section 7 presents a summary of the results and discusses how they may apply to future MGI experiments for present tokamaks and for ITER.

2. Experimental Setup, Diagnostics, Phenomenology and Metrics for Analysis

A six-valve "MEDUSA" injector [4] that provides independent control of the gas pulse duration, t_{inj}, injected gas quantity, Q, and gas delivery waveform, i.e., $Q(t)$ is used. Open/close times for each valve are ~0.2 ms and t_{inj} for low-Z gases is typically ≤ 2 ms. A 4-chord CO_2 interferometer allows accurate dynamic measurement of the very-high line-average electron densities, $\bar{n}_e$, obtained. The same MGI phenomenology, fast shutdown sequence and lack of neutral penetration beyond the separatrix seen in previously-reported single-valve MGI studies in DIII-D [5–7] are observed. Short-pulse gas delivery under conditions where $Q(t)$ is now less restricted by injection tube rise time (~10 ms for experiments reported in [7]) results in appreciably faster onset of thermal collapse and plasma current (I_p) decay. Total shutdown times, from valve opening to end-of-I_p, are now as short as 8 ms. About 2 ms is owed to the gas-sound-speed "flight time" from the valves to the plasma surface. Figures 1 and 2 show waveform data and the target plasma for the two highest-Q helium examples obtained.

Unless noted otherwise, data are obtained with an "ITER-similar" ELMy H-mode lower-single-null D_2 target plasma, with $I_p = 1.30$ MA,
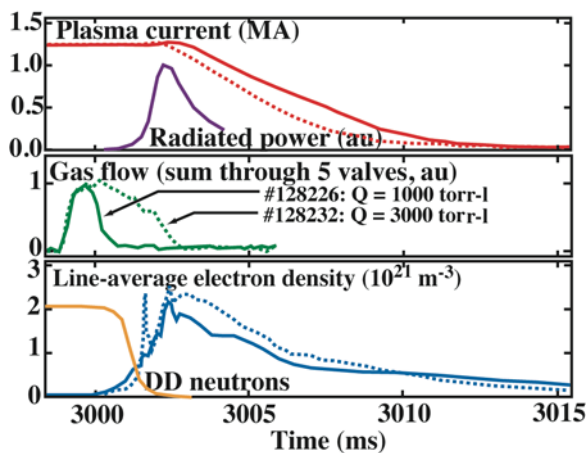

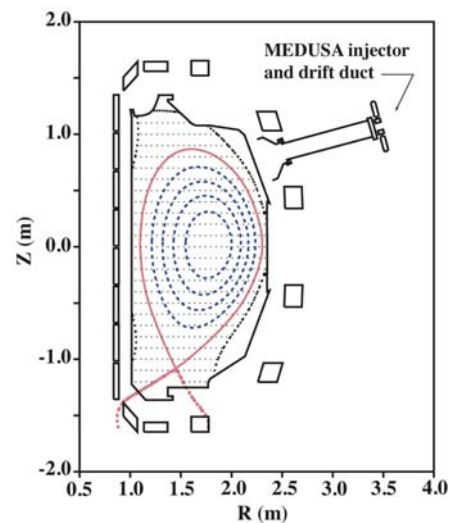FIG. 1. Two high-density fast shutdowns obtained with massive helium injection.

FIG. 2. Target plasma equilibrium (#128226) with MEDUSA injector.

R_o = 1.70 m, a = 0.60 m, q_{95} ~3.6, κ_x = 1.62 and $\delta_{u/l}$ = 0.15/0.42. Here κ_x and $\delta_{u/l}$ respectively denote the separatrix elongation and upper/lower separatrix triangularities. Plasma thermal energies, W_{th}, obtained with neutral beam heating, are typically about 0.7 MJ. Plasma magnetic energies, W_{mag}, internal to the poloidal field coil boundary, total about 1.5 MJ (0.9 MJ internal to the plasma). Average toroidal current densities are 0.7 MA/m^2 (*cf* ~0.7 MA/m^2 for ITER at 15 MA). Table I summarizes the gas species, quantities and equivalent "square-pulse" valve-open duration ranges for the 40 MGI examples interpreted here. Two ohmically-heated and three L-mode examples are included among the data. Instances where these target variations affect the fast shutdown attributes and discussion of how the "long-pulse" aspects of the injection affect the results follow.

TABLE I. Injection parameters and notes for MEDUSA MGI experiments

Species	Q (torr-l)	N_{inject} (10^{22})	Number of valves	t_{inj} (ms)	Number of examples	Note
H_2	320–2000	1.1–7.1	1–6	0.52–1.25	7	
H_2	1200–1500	4.2–5.3	1	3.8–4.9	2	"Long pulse"
H_2 + 2% Ar	2700	9.6	5	1.74	1	
D_2	420–1200	1.5–4.2	1, 2, 4, 6	1.00–2.10	4	
D_2 + 2% Ne	720–1600	2.5–4.1	2, 4, 6	1.33–1.80	2	
D_2 + 5% Ne	460–2000	1.6–7.1	2, 4, 6	0.81–1.67	3	
He	240–1000	0.85-3.5	1–5	0.95–1.25	5	1 L-mode
He	3000	1.06	5	2.86	1	"Long pulse"
Ne	120–1100	0.42–3.9	1–4, 6	1.09–1.82	6	
Ar	50–500	0.18–1.8	1–3, 5, 6	0.71–2.38	4	2 OH, 2 L-mode
Ar	900–1300	3.2–4.6	3, 6	4.3–6.2	3	"Long pulse"

All of the MEDUSA examples share a common phenomenology. Figure 3 shows the event sequence and metrics relevant to the analysis and interpretations that follow. There are three distinct phases: 1) gas delivery and edge "fueling", with edge accumulation of the entrained ions and electrons, 2) a brief period of strong MHD activity and internal magnetic reconnection that effects a more-or-less global degree of "MHD mixing" and rapid central thermal energy outflow to the radiating edge, and 3) a rapid current decay that is accompanied by a downward-going vertical instability of the current channel. Event times are determined from fast (~50 µs resolution) $I_p(t)$ and $\bar{n}_e l(t)$ [line-integral density] waveforms. These data, coupled with valve reservoir loss measurements of Q, are sufficient to quantify the time scales of the shutdown sequence and to make estimates of the resulting free electron density and in-plasma gas assimilation at, or shortly after onset of the I_p decay. Key parameters are: i) "thermal collapse" (TC) onset time, $\Delta t_{TC} = t_{TC\text{-}onset} - t_{first\text{-}gas}$, where $t_{first\text{-}gas}$ is the arrival of the first increment of gas at the plasma surface, ii) normalized "current contraction" magnitude, $I_p*(-) = I_{p,min}/I_{p0}$, for the slow I_p decay that precedes onset of the thermal collapse, and iii) the subsequent normalized "current expansion" magnitude, $I_p*(+) = I_{p,max}/I_{p,min}$. The fourth parameter, the average rate of
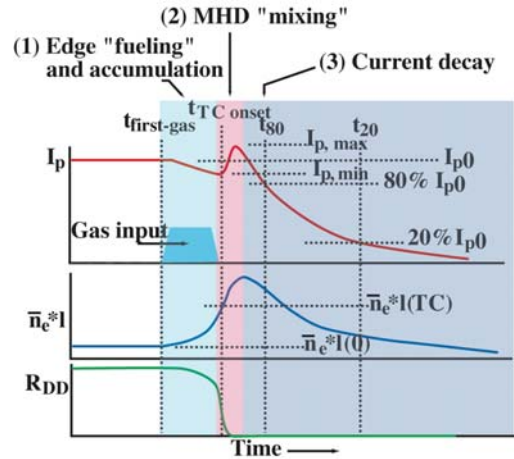

FIG. 3. Schematic MGI waveforms, events and metrics. Variations in the I_p waveform are exaggerated for clarity. Compare to Fig. 1.

current decay, $t_{CQ} = 5/3*(t_{20} - t_{80})$, provides a metric for the I_p decay. Here t_{80} and t_{20} are the times for I_p to decay to 80% and 20% of the initial before-injection plasma current I_{p0}. The t_{CQ} metric is used to interpret of the I_p decay attributes of natural disruptions that comprise the multi-tokamak International Disruption Database (IDDB) [8].

3. Thermal Energy Mitigation

With sufficient Q, fast (within 1.5–2 ms) onset of thermal-collapse radiative dissipation [5] of the plasma thermal energy ($W_{th} = ~0.7$ MJ) is obtained for all species. As Fig. 1 demonstrates, most of the dissipation occurs during a ~1-ms period that coincides with the disruption-like I_p "spike" that indicates onset of internal magnetic reconnection and broadening of the current profile. Collapse of the central plasma temperature and DD neutron emission correlates, within ~±100 μs, with the I_p-spike rise detected by fast measurements of $I_p(t)$. Hence, onset time of the I_p spike provides a "magnetic" indication of the onset of thermal collapse.

Bolometric tomography [9] shows that the principal radiation comes from a shallow region near the plasma edge, and that the main-plasma radiation is more-or-less uniform toroidally. While there are clear indications, especially for high-Z injection, of significant 3-D and 2-D localization effects during the initial impurity influx/uptake phase, the relative symmetry of the principal radiated power and coincidence of the radiation peak with the I_p spike show that the dynamics of the thermal collapse phase is mediated by a rapid outflow of central plasma energy initiated by rapid growth of internal global MHD activity [7]. Estimated time-weighted first-wall energy loadings, $W_{th}/(A_{FW}*t^{0.5})$, are ~0.3 MJ-m^{-2} s$^{-0.5}$, well short of the melting/ablation thresholds for a carbon or metallic wall. While area-normalized energy loadings obtained in DIII-D experiments fall well short of ITER loadings, the relatively good spatial uniformity and lack of excessive time peaking support the feasibility of obtaining benign radiative thermal energy dissipation in ITER. Detailed presentation of the bolometric data and radiation attributes of MEDUSA fast shutdowns is found in [9].

Figure 4 demonstrates that with sufficient Q, Δt_{TC} reaches a species-independent minimum of ≈2 ms. Exceptions to this conclusion about species-independent "saturation" include two faster-onset examples for Ar into ohmically-heated plasmas, and indications of a further modest reduction of onset time for mixed gases relative to their pure-gas counterparts. However, the limited variation in the mixed-gas parameters and number of examples make speculation with regard to Δt_{TC} for higher-Q and/or higher-concentration mixed-gas MGI premature.

FIG. 4. Thermal collapse onset times for MEDUSA MGI.

Figure 5 shows the effect of species and Q on the current profile contraction and expansion indicators. Data from past DIII-D experiments with slower-rise single-valve "open-valve" (OV) and "high-intensity" (HI) injectors (described respectively in [6] and [7]) are included for comparison. While a wide range of contraction and expansion indicators and the "expansion/contraction" ratio $R = [I_p*(+) - 1]/[1- I_p*(-)]$ are obtained in both past and present experiments, tendencies for MEDUSA to produce lower same-species and global contraction parameters and for both contraction and expansion factors to decrease with increasing Q are evident. Note the high-Q He and D_2 and H_2 mixed-gas examples, which have indicators in the range $0.97 \leq I_p*(-) \leq 0.99$ and $1.05 \geq I_p*(+) \geq 1.01$. Onset of global current decay in these
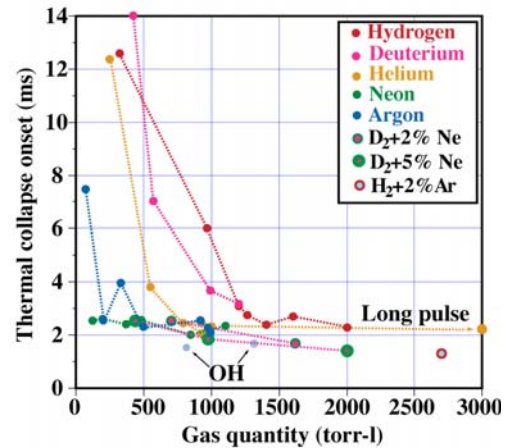
examples proceeds with only minimal current profile contraction and subsequent MHD-reconnection broadening.

Figures 4 and 5 collectively demonstrate that the $j(r)$ contraction attributes (a measure of current channel contraction owed to initial influx of impurities and/or hydrogen), the thermal quench onset time, and the subsequent $j(r)$ expansion owed to internal magnetic reconnection are ultimately approximately independent, with sufficient Q, of gas species and injection rate. These asymptotic behaviors suggest that magnetic rather than thermal diffusion in the edge sets the time-scale for the onset of the global MHD instability that effects "magnetic mixing" of the plasma core and edge regions [10], with subsequent onset of the I_p-spike-coincident thermal energy radiation pulse. Simulating these details of past and MEDUSA MGI provides a significant challenge to emerging 2D + t coupled MHD and radiation models [10,11]. The behaviors exhibited in Figs. 4 and 5 are inconsistent with the hypothesis that the inward propagation velocity of the radiation-produced "cold front" is some approximately constant fraction of the injected gas sound speed. The assimilation data presented below (Sec. 6) also show that simple constant-fraction assumptions about gas mixing ratios will not reproduce the species, mixture and Q-dependencies of the MEDUSA data.

4. Current Decay

High-Q MGI in DIII-D consistently produces a fast I_p decay. With sufficient Q, poloidal cross-section normalized current decay times [8], t_{CQ}/S, for MEDUSA MGI reach minimum values that are 3.5–4.5 ms/m^2 for He and 2.5-3.5 ms/m^2 for
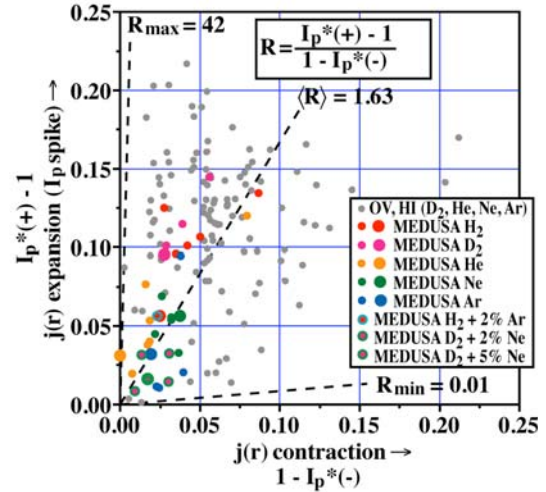

FIG. 5. Current profile contraction and expansion indicators for DIII-D MGI. For MEDUSA, large-diameter symbols denote the highest Q data for each pure gas. Grey data points are for "open-valve" and "high-intensity" DIII-D MGI [6,7].
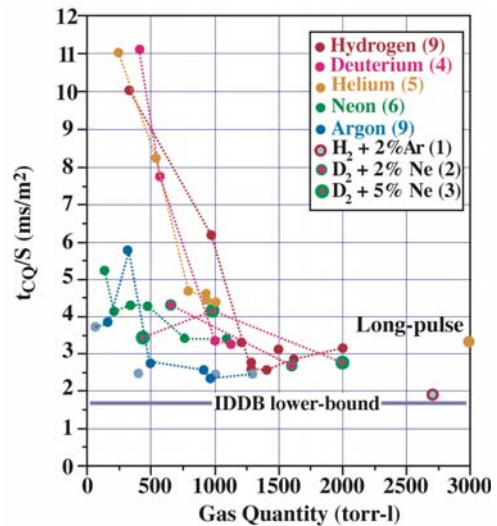

FIG. 6. Area-normalized current quench times for MEDUSA MGI. To convert to decay times, multiply by $S = \sim 1.9$ m^2.

all other gases (Fig. 6). The fastest decays are 1.5–2.5 times slower than the fastest decays (~ 1.7 ms/m^2) obtained in natural DIII-D disruptions. Fast MGI decays in DIII-D with $t_{CQ}/S \leq \sim 6$ ms/m^2 are well-correlated with substantial reduction of the vacuum vessel vertical displacement owed to vertical force impulse (Fig. 7) and (by inference) halo currents; hence we infer that all high-Q low-Z and high-Z MEDUSA examples provide effective mitigation of halo currents. The need for a relatively fast current decay to ensure vessel force and halo current mitigation in ITER is already well-recognized: note in Fig. 7 the high vessel impulse indications for "low-Q" H$_2$, D$_2$ and He MGI and for severe "natural" unmitigated vertical displacement events (VDEs) and vertically-unstable disruptions (VUDs).

5. Added Electron Density and Runaway Electron Production

Very high total electron densities, $\geq 10^{22}$ m^{-3} at, or shortly after onset of the current decay are required to guarantee mitigation of the Coulomb avalanche. The simple model invoked by Rosenbluth [1] shows that the total "no-avalanche" electron density, $n_{RB}(10^{20}$ m$^{-3}) = 8\,E$(V/m), where E is the in-plasma electric field, is ~4×10^{22} m^{-3} for both DIII-D and ITER MGI under conditions where t_{CQ}/S approaches 2 ms/m^2 (e.g., Fig. 6). The maximum $\bar{n}_e l$ obtained at CQ onset in MEDUSA experiments ranges from 2×10^{21} m^{-2} for Ne and Ar to 5–7$\times10^{21}$ m^{-2} for

FIG. 7. Area-normalized current decay times and vacuum vessel vertical impulse metric for MEDUSA MGI and "natural" disruptions and VDEs.

He, D$_2$+2% Ne and H$_2$+2% Ar (Fig. 8). When the at-CQ-onset plasma configuration, likely impurity ionization states and the corresponding I_p decay rates are taken into account, peak n_e for Ne or Ar and He/H$_2$+Ar are respectively estimated to be about 6×10^{20} m^{-3} and 2×10^{21} m^{-3}, and n_e(total)/n_{RB} ratios are 8%–10% for He and 2%–8% for other species (Fig. 9). There is no significant difference between same-Q H$_2$ or D$_2$ injection. Hydrogen/deuterium, helium and D$_2$+ 2% Ne show a favorable (~$Q^{1+\varepsilon}$) scaling of $\bar{n}_e l$ with increasing Q. Other species, including Ne, Ar and D$_2$ + 5% Ne, exhibit onset or attainment of "saturation" of $\bar{n}_e l$ (~Q^0 scaling) in their high-Q regimes.

Low levels ($\leq$ ~10 kA) of well-confined runaways that persist until closed core flux surfaces are lost near the end of the current decay are sometimes observed for high-Q Ne and Ar (9/14 examples). Subsequent single-valve experiments with ~300 torr-l neon injection have confirmed the runaway production tendencies for high-Z MGI shown in Fig. 9. All other MEDUSA fast shutdown examples are apparently runaway free.
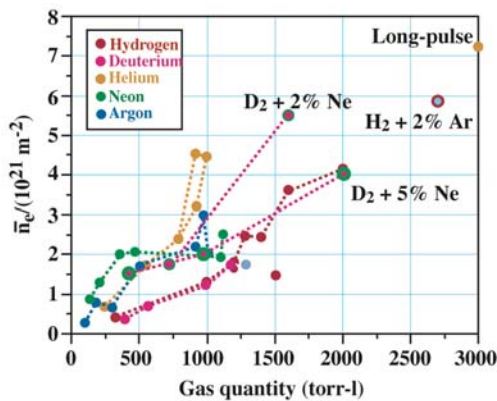

FIG. 8. Line-integral density ("v2" interferometer chord) increments for MEDUSA MGI.
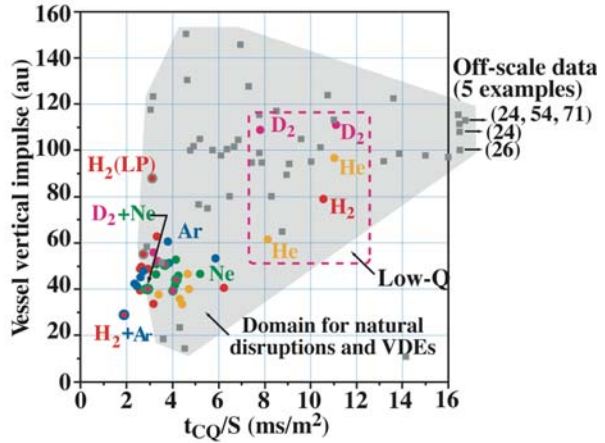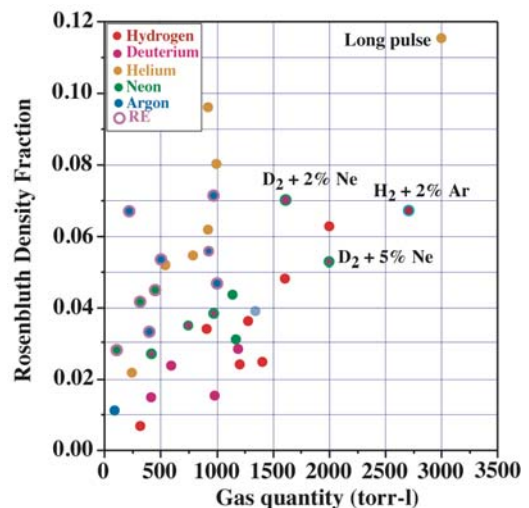

Fig. 9. Rosenbluth density fractions for MEDUSA MGI. Violet "RE" umbra denotes denotes examples with runaway electron production.

6. Gas Assimilation and Limits on Injection Duration

The six-valve He or D_2 injection capability of MEDUSA is 1.3×10^6 torr-l/s (1.7×10^5 Pa-m³/s = 300 g/s). Hence a 2-ms pulse can deliver 2500 torr-l = 0.6 g of He or D_2. Past single-valve MGI experiments in DIII-D with slower-rise injectors demonstrate that only small fractions (≤ 0.1) of high-Z gases injected were actually assimilated (entrained in ionized form) in the plasma at, or soon after onset of I_p decay [7]. Similarly finite assimilation fractions ($f_{assim} = N_{ion}/N_{gas}$) are observed for the faster-rise, higher-Q MEDUSA pulses. However, the assimilation behaviors for low-Z and high-Z injection are quite different, and whether the injection pulse length is >2 ms or <2 ms is also important. For low-Z gases, helium provides the highest assimilation (Fig. 10): f_{assim} approaches 40% and increases with increasing Q, whereas same-Q pure H_2 and D_2 assimilations are appreciably lower, albeit with a favorable ($\sim Q^1$) quantity scaling. The behavior of mixed D_2 + Ne is complex and dependant on the neon mixture. A 2% "weak" mixture significantly improves assimilation (and hence yields higher n_e) relative to pure D_2; a 5% "strong" mixture provides higher assimilation at modest Q, but assimilation falls below pure H_2 or D_2 levels at higher Q. The decline in assimilation for higher-Q D_2 + 5% Ne is similar to the assimilation behavior exhibited by pure neon (Fig. 11). Here, for pure neon or argon, the higher-Q assimilations are 0.1–0.2, albeit with what appears to be a different low-Q scaling behavior. In the "high-Q" regime relevant to runaway avalanche mitigation, both pure neon and argon MGI provide modest assimilation fractions, with no indication of favorable Q scaling.
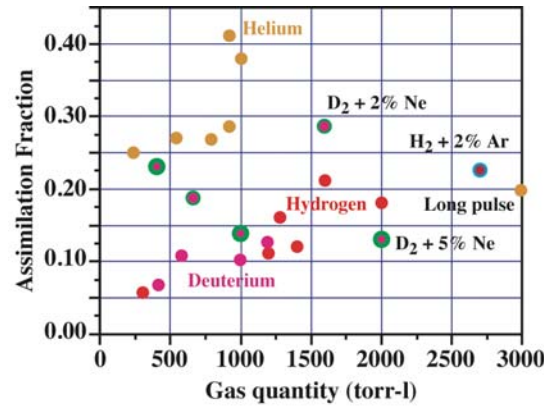

Fig. 10. Low-Z data from Fig. 9, interpreted as an assimilation fraction.

FIG. 11. High-Z data from Fig. 9, interpreted as an assimilation fraction.

The mixed D_2 + Ne assimilation behaviors shown in Fig. 10 are remarkably "nonlinear", in the sense that the increase in n_e is generally much greater than the small increment of electron content that the neon admixture provides. For example, 600 torr-l of D_2+2%Ne, which provides 8% increase in total electron input relative to 600 torr-l D_2, yields an ~80% increase in n_e and f_{assim}. A similar ~10-x "gain" in assimilation fraction relative to D_2 is obtained at low-Q for D_2+5%Ne, but the "gain" diminishes and eventually becomes negative as Q is increased. The assimilation behaviors evidenced by Fig. 10 are clearly not consistent with a simple "fixed mixing ratio" assumption about electron uptake during mixed-gas MGI.

A single long-pulse experiment with He demonstrates that gas delivered after onset of the plasma current decay is appreciably less well assimilated than gas injected before thermal collapse onset. Hence "long-pulse" He injection, with a ~3-ms duration, yields little further increase in n_e/n_{RB}. Similar indications of diminished assimilation are seen for long-pulse (> ~3 ms) H_2 and Ar injection. Given that Δt_{TC} approaches 2 ms at high Q (Fig. 4), for maximum assimilation, t_{inj} for both low-Z and high-Z gas should ideally be $\leq$ 2 ms. As Table I demonstrates, this "short-pulse" criterion is satisfied by most MEDUSA examples.

7. Summary and Conclusions

The gas injection control and variation capabilities provided by the MEDUSA injector have afforded new insight about how gas species, quantity, injection rate and high-Z impurity admixture affect the disruption mitigation and runaway avalanche suppression potential of pre-emptive MGI. With short-pulse injection and sufficient Q, all species, including pure H_2 and D_2, provide prompt (within ~2 ms) onset of benign thermal-collapse radiative dissipation of the plasma thermal energy and an ensuing fast but benign current decay with low vessel vertical force impulse and inferred reduction of in-vessel halo currents. The MEDUSA vessel impulse data explicitly confirm the well-known potential of pre-emptive MGI for ITER vessel force and halo-current mitigation and the expectation (need) for a fast current decay.

With regard to promise for achieving the very-high electron densities needed to effect collisional mitigation of runaway avalanching at, or just after onset of I_p decay, past DIII-D MGI results and MEDUSA experiments continue to show that the full "Rosenbluth density" has not yet been achieved. This is in part owing to finite in-plasma assimilation of the injected gas, and in larger part owing to the present lack of DIII-D capability to inject the large quantities (~3 g) of gas or particles required, even with full assimilation, to reach the Rosenbluth density. Overall, of the various species and mixtures tested, pure hydrogen or deuterium, helium and "weak" mixtures, e.g. D_2+2% Ne, so far exhibit the most promise for achieving n_e that will ultimately be high enough to effect avalanche mitigation at current quench onset. There are indications that the optimal neon admixture (fraction) should be decreased as the total gas quantity is increased and also clear evidence that plasma electron uptake for mixed gas MGI is not explainable in terms of a fixed-mixing-ratio hypothesis. All indications from the MEDUSA experiments support the original findings obtained by Putvinski and Rosenbuth [12] of need for 100+ g injection capabilities for ITER and a strong preference for low-Z rather than high-Z injection. Enhanced "short-pulse" mass-delivery capabilities in DIII-D and other present tokamaks are needed to test the Rosenbluth-Putvinski premise about the feasibility of effecting collisional mitigation of the runaway avalanche under conditions where an inherent "seed" population of runaway electrons exists.

Acknowledgments

References

[1]   *Chapter 3, ITER Physics Basis*, Nucl. Fusion (1999) 2253.
[2]   ROSENBLUTH, M.N., *et al.*, Nucl. Fusion **37** (1997) 955.
[3]   *Progress in the ITER Physics Basis*, Nucl. Fusion **47** (2007) S1-414.
[4]   JERNIGAN, T.C., *et al.*, Bull. Am. Phys. Soc. **52** (2007) 171.
[5]   TAYLOR, P.L., *et al.*, Phys. Plasmas **6** (1999) 1872; WHYTE, D.G., *et al.*, Phys. Plasmas **7** (2000) 4052.
[6]   WHYTE, D.G., *et al.*, J. Nucl. Mater. **313-316** (2003) 1239.
[7]   HOLLLMANN, E.M., *et al.*, Nucl. Fusion **45** (2005) 1046.
[8]   WESLEY, J.C., *et al.*, "Disruption Characterization and Database Activities for ITER," Proc. of 21st IAEA Fusion Energy Conf., Chengdu, China, 2006, Paper IT/P1-21.
[9]   HOLLMANN, E.M., *et al.*, to be published in Nucl. Fusion (2008)
[10] IZZO, V.A., Nucl. Fusion **46** (2006) 541.
[11] IZZO, V.A., *et al.*, Physics Plasmas **15** (2008) 056109.
[12] PUTVINSKI, S., *et al.*, J. Nucl. Mater. **241**-**243** (1997) 316.